Sensors and Materials, Vol. 38, No. 6 (2026) 3041–3050
MYU Tokyo

S & M 4487

Bio-based Multi-filler Poly(methyl methacrylate) Composites for Sustainable UV-protective and Low-loss Microwave Sensor Applications

Dieter Rahmadiawan,[1,2] Shih-Chen Shi,[1*] and Du-Yi Wang[1]

[1]Department of Mechanical Engineering, National Cheng Kung University (NCKU), No. 1, University Road, Tainan 70101, Taiwan
[2]Department of Mechanical Engineering, Universitas Negeri Padang, 25173 Padang, Sumatera Barat, Indonesia

(Received February 27, 2026; accepted May 25, 2026)

Keywords: PMMA composites, multi-filler synergy, UV shielding, low microwave loss, interfacial polarization

In this study, we developed multi-filler poly(methyl methacrylate) (PMMA) composites with enhanced UV shielding and low microwave loss. Integrating SiO_2, cellulose nanocrystals (CNCs), and brominated lignin (Br-lignin) effectively tuned interfacial polarization and microstructural distribution, resulting in significantly improved UV blocking performance and stable dielectric behavior at 28 and 40 GHz. The UV blocking efficiency increased from 0.20 for pristine PMMA to 0.85 and 0.82 for the SL2 and K12 systems, corresponding to enhancements of up to 325 and 310%, respectively. These improvements are attributed to the combined effects of structural scattering from SiO_2 and charge–transfer interactions from Br-lignin, which promote extended UV attenuation and enhanced light–matter interaction. Among all formulations, the ternary system achieved a balanced multifunctional performance, maintaining strong UV shielding while controlling dielectric loss through stabilized interfacial structures. In contrast, binary systems exhibited limited or sub-additive behavior due to partial interfacial interference. The results indicate that UV shielding and dielectric properties are governed by distinct but interconnected mechanisms, where scattering-dominated processes enhance optical attenuation with minimal dielectric impact, while charge–transfer interactions contribute to both UV absorption and polarization response. The integration of bio-derived fillers enhances circular economy potential and reduces reliance on purely synthetic additives. These findings provide a scalable pathway for designing environmentally responsible polymer composites with optimized optical and electromagnetic performance for advanced sensing applications.

1. Introduction

The rapid expansion of smart sensing technologies for Industry 4.0, environmental monitoring, and renewable energy systems demands advanced materials that combine optical protection, electromagnetic (EM) stability, and sustainability.[1–3] Poly(methyl methacrylate)

*Corresponding author: e-mail: scshi@mail.ncku.edu.tw
https://doi.org/10.18494/SAM6309

ISSN 0914-4935
https://myukk.org/

(PMMA) exhibits excellent optical transparency and low density, making it widely used in automotive lighting, signage, and outdoor optical components.[4] However, PMMA faces two critical functional limitations. First, its UV absorption is insufficient, resulting in photodegradation and shortened service life under long-term sunlight exposure.[5] Second, PMMA lacks effective microwave absorption, restricting its application in emerging electromagnetic (EM) shielding and sensing fields. As the demand for high-performance outdoor materials and innovative electronics continues to grow, polymer composites with simultaneous UV shielding and microwave absorption functions are attracting increasing attention. Incorporating multifunctional fillers with polar groups and EM-coupling capabilities provides a promising route to extend the functionality of PMMA.[6]

Filler reinforcement has been recognized as an effective strategy to improve polymers' UV and microwave absorption properties.[5,7–10] Previous studies have demonstrated that fillers with polar structures or EM-interactive properties modify the PMMA microstructure, enhance UV shielding, and increase dielectric loss efficiency.[11] In particular, recent studies have highlighted that interfacial polarization and filler dispersion play critical roles in determining dielectric behavior at GHz frequencies, while hybrid filler systems can enhance UV shielding through combined scattering and electronic transition mechanisms.[12–15]

Interfacial interactions, dispersion uniformity, and chemical bonding therefore strongly affect the overall absorption efficiency.[16] Since single fillers often fail to achieve multifunctionality, multi-filler composite designs have attracted research interest for achieving simultaneous optical and electromagnetic enhancements.

Among potential filler candidates, SiO_2, lignin derivatives, and cellulose nanocrystals (CNCs) offer complementary functionalities. SiO_2 contributes to UV attenuation primarily through scattering effects induced by refractive index mismatch while also facilitating interfacial polarization at high frequencies. CNCs enhance microstructural stability and provide abundant surface functional groups that promote interfacial interactions.

Moreover, brominated lignin (Br-lignin), with its aromatic and conjugated structure, enables UV absorption through π–π^* electronic transitions and charge–transfer interactions while also contributing to dipolar polarization. Despite these advantages, the combined behavior of these fillers in multi-filler systems, particularly their interaction mechanisms at GHz frequencies, remains insufficiently understood.

In this study, we aim to develop a multi-filler PMMA composite incorporating hydrolyzed SiO_2, modified Br-lignin, and CNCs. SiO_2 and CNCs provide nanoscale scattering and interfacial polarization, whereas Br-lignin contributes UV absorption through electronic transitions and dielectric loss through dipole interactions.[17–19] We hypothesize that a synergistic multi-filler network enhances UV shielding and microwave absorption, establishing a functional PMMA composite for advanced optical protection and EM shielding applications.[20]

2. Materials and Methods

2.1 Materials

Lignin (Indulin AT, Taimax, Taiwan), tetrahydrofuran (THF, Avantor, USA), α-bromoisobutyryl bromide (BiBB, Sigma-Aldrich, USA), argon (Yunhai Industrial Gas Co., Taiwan), and deionized (DI) water (Yean Hern Chemical, Taiwan) were used for brominated lignin synthesis.

Tetraethoxysilane (TEOS, 98%, Thermo Scientific, USA), ethanol (99.5%, Shin Shin Chemical Co., Taiwan), and ammonium hydroxide (NH_4OH, 25%, PanReac AppliChem, Spain) were used for silica precursor preparation.

PMMA (Sigma-Aldrich, USA), CNCs (CellForce, Canada), Br-lignin (synthesized in-house), and nano-SiO_2 suspension (synthesized in-house) were used as composite constituents.

3-(Trimethoxysilyl)propyl methacrylate (MPTS), benzoyl peroxide (BPO), copper (II) bromide ($CuBr_2$, 99%), 2,2-bipyridine, hydrochloric acid (HCl), and copper wire were used for surface modification and atom transfer radical polymerization (ATRP).

2.2 Sample preparation

Lignin (1 g) was dissolved in 50 mL of THF under ultrasonication for 20 min. The solution was transferred into a four-neck flask and degassed through three vacuum-argon cycles to establish an inert atmosphere. BiBB (0.5 mL per g lignin) was added, and the reaction proceeded at 45 ℃ for 48 h under stirring. After the reaction, DI water (threefold volume) was added to precipitate the product. The floating solid was collected, washed three times, and freeze-dried for 24 h to obtain Br-lignin.

Nano-SiO_2 was synthesized via a sol-gel process. TEOS and ethanol were mixed and stirred at 70 ℃ (200 rpm) for 10 min. DI water was added dropwise, followed by NH_3 to promote hydrolysis and condensation. For 1 g of SiO_2, the volumetric ratio TEOS:C_2H_5OH:DI water:NH_3 was 3.696:1.944:1.199:0.00512 mL (1:2:4:0.0164 mol). The resulting suspension was used directly for composite fabrication.

PMMA was dissolved in THF (1 g:5 mL) at 60 ℃ and 300 rpm. BPO (1 wt%) was added to activate grafting sites. For PMMA/SiO_2 composites, the SiO_2 suspension was surface-modified with MPTS (SiO_2:MPTS = 1 g:4.73 mL) at 70 ℃ for 2–4 h before mixing with the PMMA solution. For PMMA/Br-lignin composites, Br-lignin was dispersed in THF and reacted with PMMA via ATRP using $CuBr_2$/BPY and acid-washed copper wire under argon at room temperature for 24 h. For PMMA/CNC composites, CNCs were ultrasonically dispersed into the PMMA solution (30 min ultrasonication + 1 h stirring). Dual- and triple-filler systems were prepared by combining the corresponding procedures sequentially. In triple systems, a SiO_2/CNC suspension replaced pure SiO_2 sol where applicable. All mixtures were cast into PTFE molds, covered with perforated aluminum foil, and dried at 60 ℃ for 1–2 days.

Dried composites were ground into fine powders using a dual-stage crusher. For UV absorption testing, powders were hot-pressed at 185 ℃ under sequential pressures (1000 kgf pre-

press, 2500 kgf for 5 min, and 2600 kgf during cooling) to obtain optical sheets (1–4 cm). For microwave absorption testing, 0.35 g of powder was hot-pressed under identical conditions to produce sheets (<0.1 mm thick), which were cut into 43 mm × 35 mm rectangles. Composite codes and compositions are summarized in Table 1.

2.3 Analytical techniques

UV-Vis-NIR spectra were recorded using a HITACHI U4100 spectrophotometer over 200–600 nm to evaluate UV-blocking performance. The UV blocking efficiency (BE) was quantitatively determined on the basis of average transmittance in the UV region (200–400 nm), calculated as $BE = 1 - T_{UV}$, where T_{UV} represents the mean transmittance over the selected wavelength range. Microwave absorption properties were measured using an antenna measurement system. The dielectric constant and loss tangent were evaluated at 28 and 40 GHz to assess electromagnetic attenuation performance in single-, dual-, and triple-filler composites.

3. Results and Discussion

3.1 UV absorption of multi-filler composites

PMMA exhibited its primary high absorption band (≥90%) in the 200–250 nm range (Fig. 1). The incorporation of CNCs shifted the edge to ~245 nm, while SiO_2 extended it to ~288 nm, with C1 slightly narrowing the range by ~5 nm. This behavior results from CNCs increasing the effective refractive index and SiO_2 introducing structural scattering, altering optical paths and edge positions.[21,22]

Table 1
Codes and compositions of PMMA-based composites.

Sample code	PMMA composite description
P	Pure PMMA
Single-filler composites	
S1	SiO_2 1 wt%
S5	SiO_2 5 wt%
S10	SiO_2 10 wt%
L1	Br-lignin 1 wt%
C01	CNCs 0.1 wt%
C1	CNCs 1 wt%
C5	CNCs 5 wt%
Dual-filler composites	
SL1	SiO_2 1 wt% + Br-lignin 1 wt%
SL2	SiO_2 2 wt% + Br-lignin 2 wt%
S1C01	SiO_2 1 wt% + CNCs 0.1 wt%
SC1	SiO_2 10 wt% + CNCs 1 wt%
LC01	Br-Lignin 1 wt% + CNCs 0.1 wt%
Triple-filler composites	
K01	SiO_2 1 wt% + Br-lignin 1 wt% + CNCs 0.1 wt%
K12	SiO_2 2 wt% + Br-lignin 2 wt% + CNCs 1 wt%

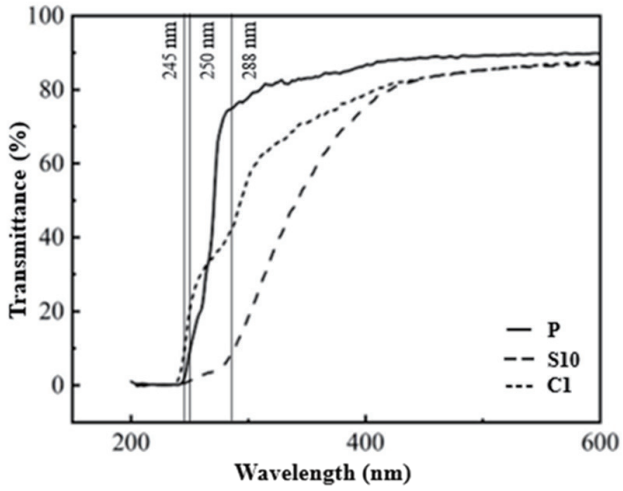

Fig. 1. UV absorption spectra of PMMA and multi-filler composites; dashed line marks the > 90% absorption range.

The binary SC1 system combined the features of S10 and C1 (Fig. 2). A sharp peak appeared near 230 nm, nearly overlapping with C1 but with greater intensity, and a broad plateau emerged across 245–288 nm, similar to S10. This synergy effect indicates that SiO_2 and CNCs form a cooperative optical shielding network that reduces UV penetration and mitigates PMMA backbone degradation.

The binary SL2 and ternary K12 systems displayed stable absorption between 200 and 400 nm (Fig. 3). Br-lignin's aromatic conjugation and SiO_2 interfaces jointly provided effective UV shielding, while K12 showed a higher intensity and a wider range extending to 417 nm. This enhancement is attributed to ternary interfacial heterogeneity, which promotes local charge-transfer states and produces a redshifted absorption edge.[23]

PMMA exhibited a baseline absorption effectiveness with a BE of 0.20 (Table 2). The incorporation of CNCs (C1) increased the BE to 0.30, corresponding to an improvement of +50% relative to PMMA, indicating a moderate enhancement due to refractive index modification. The SiO_2 system (S10) further increased the BE to 0.35 (+75%), suggesting a stronger contribution from structural scattering mechanisms.

The binary SC1 system showed a BE of 0.40, representing a +100% increase compared with pristine PMMA. However, when compared with the expected additive value of the individual components (0.30 + 0.35 − 0.20 = 0.45, corrected for baseline overlap), the observed BE is slightly lower, indicating a sub-additive interaction (~−11%). This suggests that while CNCs and SiO_2 contribute cooperatively, partial aggregation or interfacial interference may limit the full synergistic potential in the binary system.

In contrast, the SL2 system exhibited a significantly higher BE of 0.85, corresponding to a +325% enhancement over PMMA, demonstrating a substantial improvement driven by the combined effects of aromatic conjugation and interfacial scattering. The ternary K12 system achieved a BE of 0.82 (+310%), maintaining a similarly high level of UV shielding performance. Compared with the expected additive contribution from binary components, both SL2 and K12

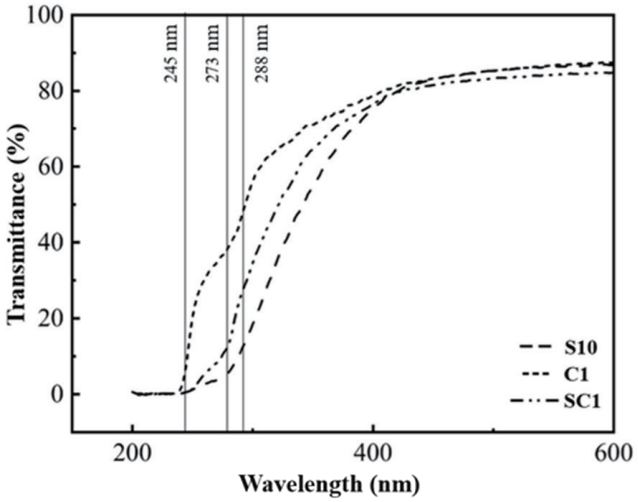

Fig. 2. UV transmittance spectra of PMMA composites with single and binary fillers (CNCs, SiO_2, and SiO_2 + CNCs).

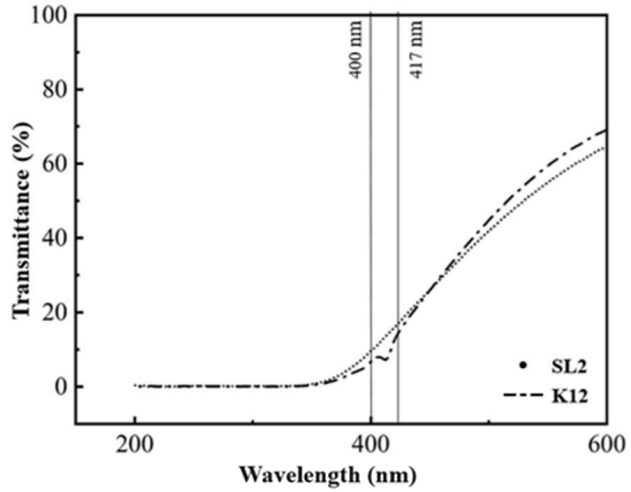

Fig. 3. UV transmittance spectra of PMMA composites with binary (SiO_2 + Br-lignin) and ternary (SiO_2 + Br-lignin + CNCs) fillers.

Table 2
UV BE values of PMMA-based composites calculated from the average transmittance in the 200–400 nm wavelength range.

Sample	BE	Insight
P	0.2	Baseline
S10	0.35	Moderate improvement
C1	0.3	Slight improvement
SC1	0.4	Improved but limited
SL2	0.85	Very high UV blocking
K12	0.82	Very high UV blocking

exhibit strong positive synergy, with effective absorption far exceeding simple linear combinations. This indicates that multi-component interfacial heterogeneity promotes enhanced light attenuation mechanisms, likely through combined electronic interactions and multi-scale scattering effects.

3.2 Dielectric properties at 28 and 40 GHz

Figures 4 and 5 show the dielectric constant and loss tangent (tan δ) of pure PMMA and its composites at frequencies of 28 and 40 GHz, respectively. S1 (1 wt% SiO_2) reached a dielectric constant of ~3.7, while S5 (5 wt% SiO_2) was slightly above pure PMMA. Low SiO_2 content dispersed uniformly and stabilized interfacial polarization, whereas high loading promoted agglomeration that reduced effective polarization.[24] Br-lignin and CNCs alone contributed minimally at high frequencies, as their polar groups respond slowly to rapid field oscillations.[25,26]

SL1 (SiO_2 + Br-lignin), S1C01 (SiO_2 + CNCs), and K01 (ternary) showed slightly lower dielectric constants than S1. Additional fillers disturbed the stable SiO_2 interfacial network,

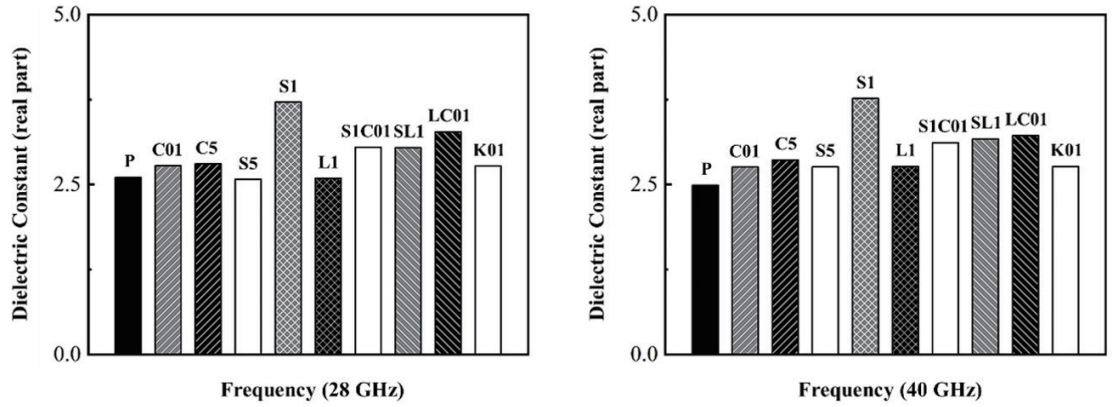

(a) (b)

Fig. 4. Dielectric constant values of pure PMMA and composites at (a) 28 and (b) 40 GHz.

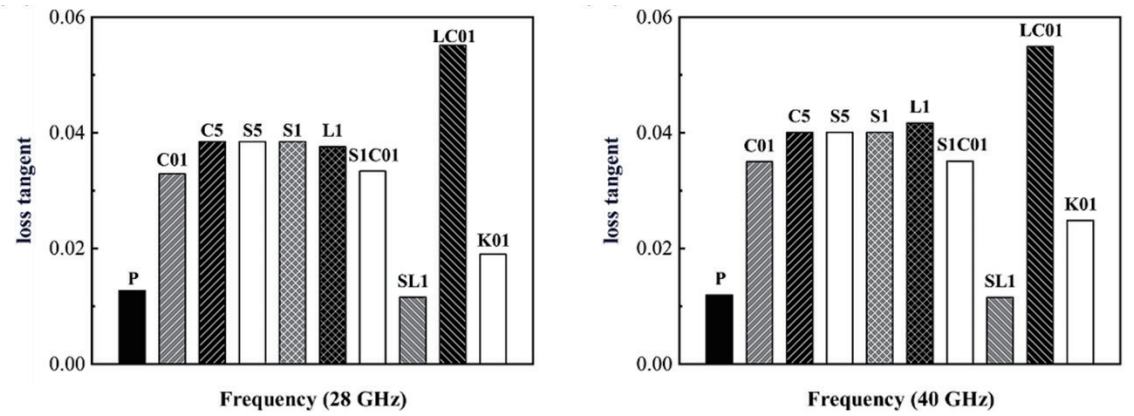

(a) (b)

Fig. 5. Loss tangent (tan δ) values of pure PMMA and composites at (a) 28 and (b) 40 GHz.

creating partial incompatibility that weakened polarization efficiency. Single Br-lignin or CNC additions remained near the permittivity of neat PMMA, confirming their limited contribution at GHz frequencies.

As shown in Fig. 5, LC01 (Br-lignin + CNCs) produced the highest loss tangent (tan δ) owing to loose, discontinuous interfaces where local field distortion generated energy dissipation.[27] SL1, with chemically anchored and well-dispersed fillers, had the lowest loss, and K01 showed only a slight increase in tan δ due to effective ternary synergy. S5 maintained a tan δ similar to that of S1 because SiO_2, as a low-loss filler, does not promote strong dipole oscillation even under partial clustering.[28]

The UV shielding and dielectric behavior are governed by distinct but interconnected mechanisms. SiO_2 primarily contributes through scattering effects due to refractive index mismatch, enhancing UV attenuation without significantly increasing dielectric loss. In contrast, Br-lignin introduces π-π* electronic transitions and charge–transfer interactions, which extend UV absorption into the visible range while also contributing to dipolar polarization.

The combination of these fillers in ternary systems creates a balance between scattering-dominated and charge-transfer-dominated mechanisms, resulting in broadened UV absorption and controlled dielectric loss.

4. Conclusions

We developed multi-filler PMMA composites with enhanced UV shielding and low dielectric loss at microwave frequencies, demonstrating that complementary fillers can be strategically combined to achieve balanced multifunctional performance. The results showed that UV attenuation is primarily governed by the combined effects of structural scattering (SiO_2) and charge–transfer interactions (Br-lignin), while the dielectric response at 28–40 GHz is dominated by interfacial polarization and localized charge displacement, resulting in stable low-loss behavior.

From an engineering perspective, the findings provide a clear design guideline: low-loss dielectric materials with strong UV shielding can be achieved by integrating fillers with distinct but complementary roles while carefully controlling filler loading and interfacial structure to avoid excessive dielectric dissipation. The ternary system K01 demonstrates that optimized filler interactions can suppress dielectric loss while maintaining high UV blocking performance, which is critical for applications requiring signal stability.

These materials are particularly suitable for protective encapsulation layers, low-loss substrates, and structural components in high-frequency sensing and electronic systems exposed to outdoor environments. The use of bio-derived fillers further enhances sustainability without compromising functional performance. Overall, this work offers a scalable engineering strategy for designing lightweight polymer composites with controlled optical and electromagnetic properties for next-generation smart devices.

Acknowledgments

The authors gratefully acknowledge the Core Facility Center at National Cheng Kung University, Taiwan, for providing access to the EM000800 and SQUID000200 instruments, which were funded by the NSTC project 114-2740-M-006-001. Additional support from the Higher Education Sprout Project of the Ministry of Education, Taiwan, through the Headquarters of University Advancement at National Cheng Kung University (NCKU), is also gratefully acknowledged.

References

1 M. Anwar, H. Hidayat, and E. Sabrina: TEM J. **12** (2023) 1719. https://doi.org/10.18421/tem123-54
2 S. Roseno, M. I. Ammarullah, S. Rohman, F. Kurniawati, T. Wahyudi, A. H. S. Wargadipura , M. Masmui, D. Budiyanto, M. D. Effendi, W. Wahyudin, E. Kalembang, H. Hernawan, S. Subari, S. Habibie, T. P. H. Simanjuntak, H. Santoso, A. Ahmad, and A. L. Juwono: AIP Advances **14** (2024) 015044. https://doi.org/10.1063/5.0183153
3 N. Yuniarti, Y. Rahmawati, M. Anwar, V. G. Al Hakim, H. Hidayat, D. Hariyanto, A. F. Husna, and J.-H. Wang: Eur. J. Educ. **59** (2024) e12725. https://doi.org/10.1111/ejed.12725
4 D.-Y. Wang, S.-C. Shi, and D. Rahmadiawan: J. Polym. Mater. **42** (2025) 1075. https://doi.org/10.32604/jpm.2025.072263
5 Kadriadi, D. Rahmadiawan, H. Abral, Ilhamdi, M. Ivan, Akmal, D. Handayani, L. R. Septria Ningrum, R. S. Masri, B. A. Widyaningrum, M. H. Mohamad Kassim, and M. Mahardika: Food Biosci. **68** (2025) 106500. https://doi.org/10.1016/j.fbio.2025.106500
6 J. Guo, Y. Wang, L. Wang, B. Ding, Y. Wang, Y. Sun, S. Dai, D. Wang, and S. Bi: Materials **17** (2024) 5427.
7 M. I. Ammarullah, I. Y. Afif, M. I. Maula, T. I. Winarni, M. Tauviqirrahman, and J. Jamari: Mater. Today: Proc. **63** (2022) S143. https://doi.org/10.1016/j.matpr.2022.02.055
8 R. Saravanan, S. J. Arunachalam, T. Sathish, J. Giri, and M. I. Ammarullah: Eng. Rep. **7** (2025) e13059. https://doi.org/10.1002/eng2.13059
9 T.-T. Huang, D. Rahmadiawan, and S.-C. Shi: J. Materi. Res. Technol. **32** (2024) 1460. https://doi.org/10.1016/j.jmrt.2024.08.003
10 Y.-T. Chen, S.-C. Shi, and D. Rahmadiawan: Sens. Mater. **37** (2025) 1835. https://doi.org/10.18494/sam5447
11 J. Salla, K. K. Pandey, and K. Srinivas: Polym. Degrad. Stab. **97** (2012) 592.
12 M. Samet, A. Kallel, and A. Serghei: J. Compos. Mater. **56** (2022) 3197. https://doi.org/10.1177/00219983221090629
13 R. R. Henriques, A. Schettini, and B. G. Soares: J. Compos. Sci. **10** (2026) 50. https://doi.org/10.3390/jcs10010050
14 D. Gasni, D. Rahmadiawan, R. Irwansyah, and A. E. Khalid: Lubricants **12** (2024) 78. https://doi.org/10.3390/lubricants12030078
15 D. Rahmadiawan, T. F. Santos, N. Aslfattahi, S.-C. Shi, E. Indrawan, A. Ramadhan, and Z. Abadi: Teknomekanik **8** (2025) 252. https://doi.org/10.24036/teknomekanik.v8i2.44072
16 S.-C. Shi, X.-N. Tsai, and D. Rahmadiawan: Surf. Coat. Technol. **483** (2024) 130712. https://doi.org/10.1016/j.surfcoat.2024.130712
17 F. Cao, J. Xu, X. Zhang, B. Li, X. Zhang, Q. Ouyang, X. Zhang, and Y. Chen: Nanomaterials **11** (2021) 2636. https://doi.org/10.3390/nano11102636
18 M. Lin, L. Yang, H. Zhang, Y. Xia, Y. He, W. Lan, J. Ren, F. Yue, and F. Lu: Ind. Crops and Prod. **174** (2021) 114212. https://doi.org/10.1016/j.indcrop.2021.114212
19 Z. Du, C. Zhou, H. Zhang, and R. Zhao: Mater. Lett. (2025) 138215. https://doi.org/10.1016/j.matlet.2025.138215
20 C. Vallés, D. G. Papageorgiou, F. Lin, Z. Li, B. F. Spencer, R. J. Young, and I. A. Kinloch: Carbon **157** (2020) 750. https://doi.org/10.1016/j.carbon.2019.10.075
21 S. Liu, M. D. Islam, Z. Ku, D. A. Boyd, Y. Zhong, A. M. Urbas, E. Smith, J. Derov, V. Q. Nguyen, W. Kim, J. S. Sanghera, Y. Ko, J. Genzer, X. Ye, Z. Guo, E. Seo, and J. E. Ryu: Composites, Part B **223** (2021) 109128. https://doi.org/10.1016/j.compositesb.2021.109128
22 D. Pratap, Vikas, R. Gautam, A. K. Shaw, and S. Soni: Colloids Surf., A **635** (2022) 128054. https://doi.org/10.1016/j.colsurfa.2021.128054

23 X. Wu, H. Lian, and X. Li: J. Cleaner Prod. **430** (2023) 139694. https://doi.org/10.1016/j.jclepro.2023.139694
24 L. Padurariu, E. Brunengo, G. Canu, L. P. Curecheriu, L. Conzatti, M. T. Buscaglia, P. Stagnaro, L. Mitoseriu, and V. Buscaglia: ACS Appl. Mater. Interfaces **15** (2023) 13535. http://dx.doi.org/10.1021/acsami.2c23013
25 M. H. A. Rehim and G. M. Turky: Results in Surf. Interfaces **17** (2024) 100324. https://doi.org/10.1016/j.rsurfi.2024.100324
26 Q. Wang, J. Che, W. Wu, Z. Hu, X. Liu, T. Ren, Y. Chen, and J. Zhang: Polymers **15** (2023) 590. https://doi.org/10.3390/polym15030590
27 H. Shen, X. Shi, Z. Wang, P. Zou, Z. Hou, C. Xu, L. Zhang, and H. Wu: Metals **12** (2022) 2154. https://doi.org/10.3390/met12122154
28 B. Huang, Y. Yu, Y. Zhao, Y. Zhao, L. Dai, Z. Zhang, and H.-F. Fei: ACS Omega **8** (2023) 35275. https://doi.org/10.1021/acsomega.3c05066